Journal of Geophysical Research: Solid Earth

RESEARCH ARTICLE
10.1029/2018JB016136

Key Points:
- Offshore tectonic tremor localizes at subducted seamounts during and immediately following the 2014 Gisborne SSE
- Stresses from seamount subduction dominate megathrust slow slip in producing seismicity and tremor
- A wide range of slip processes occur on the plate interface in very close proximity to one another

Supporting Information:
- Figure S1

Correspondence to:
E. K. Todd,
erin.todd@otago.ac.nz

Citation:
Todd, E. K., Schwartz, S. Y., Mochizuki, K., Wallace, L. M., Sheehan, A. F., Webb, S. C., et al. (2018). Earthquakes and tremor linked to seamount subduction during shallow slow slip at the Hikurangi Margin, New Zealand. *Journal of Geophysical Research: Solid Earth*, *123*, 6769–6783. https://doi.org/10.1029/2018JB016136

Received 22 MAY 2018
Accepted 20 JUL 2018
Accepted article online 27 JUL 2018
Published online 20 AUG 2018

Earthquakes and Tremor Linked to Seamount Subduction During Shallow Slow Slip at the Hikurangi Margin, New Zealand

Erin K. Todd[1,2], Susan Y. Schwartz[1], Kimihiro Mochizuki[3], Laura M. Wallace[4,5], Anne F. Sheehan[6], Spahr C. Webb[7], Charles A. Williams[4], Jenny Nakai[6], Jefferson Yarce[6], Bill Fry[4], Stuart Henrys[4], and Yoshihiro Ito[8]

[1]Department of Earth and Planetary Sciences, University of California, Santa Cruz, CA, USA, [2]Now at Department of Geology, University of Otago, Dunedin, New Zealand, [3]Earthquake Research Institute, University of Tokyo, Tokyo, Japan, [4]GNS Science, Lower Hutt, New Zealand, [5]University of Texas Institute for Geophysics (UTIG), Austin, TX, USA, [6]Cooperative Institute for Research in Environmental Sciences, University of Colorado Boulder, Boulder, CO, USA, [7]Lamont-Doherty Earth Observatory (LDEO), Columbia University, New York, NY, USA, [8]Disaster Prevention Research Institute, Kyoto University, Kyoto, Japan

Abstract Shallow slow slip events have been well documented offshore Gisborne at the northern Hikurangi subduction margin, New Zealand, and are associated with tectonic tremor downdip of the slow slip patch and increases in local microseismicity. Tremor and seismicity on the shallow subduction interface are often poorly resolved due to their distance from land-based seismic and geodetic networks. To address this shortcoming, the Hikurangi Ocean Bottom Investigation of Tremor and Slow Slip experiment deployed 24 absolute pressure gauges and 15 ocean bottom seismometers on the seafloor above the Gisborne slow slip patch to investigate the spatial and temporal extent of slow slip and associated tremor and earthquake activity. We present a detailed spatiotemporal analysis of the seismic signatures of various interplate slip processes associated with the September/October 2014 Gisborne slow slip event. Tectonic tremor begins toward the end and continues after the geodetically constrained slow slip event and is localized in the vicinity of two subducted seamounts within and updip of the slow slip patch. The subsequent, rather than synchronous occurrence of tremor suggests that tremor may be triggered by stress changes induced by slow slip. However, Coulomb failure stress change models based on the slow slip distribution fail to predict the location of tremor, suggesting that seamount subduction plays a dominant role in the stress state of the shallow megathrust. This and the observed interplay of seismic and aseismic interplate slip processes imply that stress changes from slow slip play a secondary role in the distribution of associated microseismicity.

1. Introduction

Slow slip events (SSEs) are now recognized as an important part of the spectrum of strain release processes ranging from steady aseismic plate convergence rates of a few centimeters per year to regular earthquakes with fault slip rates of a few meters per second (e.g., Beroza & Ide, 2011; Peng & Gomberg, 2010; Schwartz & Rokosky, 2007). Over the last decade, the list of regions with documented slow slip events has increased and diversified. Slow slip and related seismic phenomena have been identified in numerous subduction margins around the globe (e.g., Douglas et al., 2005; Dragert et al., 2001; Hirose & Obara, 2005; Jiang et al., 2012; Kostoglodov et al., 2003; Obara et al., 2004; Ohta et al., 2006; Outerbridge et al., 2010; Radiguet et al., 2016; Vallée et al., 2013; Wallace & Beavan, 2010). The abundant observations of slow slip have shown that it occurs under a variety of depth and temperature conditions and exhibits a wide range of behaviors in magnitude, duration, recurrence interval, and association with tremor and/or microseismicity. While slow slip at many subduction margins occurs at depths of 30–50 km, slow slip along the northern Hikurangi Margin, New Zealand; the Nicoya Peninsula, Costa Rica; the Boso Peninsula, Japan; and near La Plata Island, Ecuador, is shallow (e.g., Ozawa et al., 2003; Protti et al., 2004; Vallée et al., 2013; Wallace & Beavan, 2010), occurring at depths of less than 15 km, and often in locations where margin tectonics are dominated by the subduction of seamounts and ridges (see review in Saffer & Wallace, 2015).

While the exact physical mechanisms for slow slip are not well understood, it is accepted that slow slip is a manifestation of shear failure, like a regular earthquake, but with a considerably slower slip speed

controlled by some other process such as dilatant hardening (Segall et al., 2010), transitional frictional behavior from high fluid pressures (Liu & Rice, 2007), rate-dependent changes in frictional properties (from velocity weakening to velocity strengthening) with increasing slip speed (Kaproth & Marone, 2013; Shibazaki & Iio, 2003), or the evolution of elastic stiffness in a localized shear fabric (Leeman et al., 2015). The coincidence of shallow slow slip with regions where subduction of topographically high features like seamounts and ridges have thoroughly fractured the upper plate (Dominguez et al., 1998; Ruh et al., 2016; Wang & Bilek, 2011, 2014) suggests that slow slip can be enhanced by heterogeneity of plate boundary properties. In this case (and perhaps others), we expect slow slip to be accommodated on a network of fractures, rather than along a single plane.

A large proportion of the existing slow slip observations in subduction zones come from regions where slow slip occurs at depths of 20–50 km—typically beneath the land and thus (relatively) easily instrumented (e.g., Dragert et al., 2001; Hirose et al., 1999; Kostoglodov et al., 2003), enabling numerous observations and good characterization of slip. The behavior of the shallow, offshore portion of the subduction interface is, however, often poorly resolved. Regions such as Costa Rica, New Zealand, Ecuador, and the Boso Peninsula, Japan, where land is close to the trench and slow slip has been documented at shallow ($<$15 km) depths, provide a special opportunity to observe and quantify the behavior and conditions in the very near-field of slow slip. Additionally, the presence of subducted seamounts in each of these locations provides an opportunity to directly address the role that seafloor roughness plays in aseismic slow slip and its associated seismic phenomena like low-frequency earthquakes, or tremor. Although the influence that subducting seamounts and related high topography have on interplate behavior is controversial, recent reviews suggest that subducting high relief is more frequently associated with low seismic coupling and aseismic creep than with large megathrust earthquake failure (see Wang & Bilek, 2014 for a review). Most models of megathrust locking are derived from seismic and geodetic observations made on land and suffer from the same problem of poor offshore resolution as models of shallow slow slip. Instrumenting the seafloor provides a window into the range of slip processes occurring on and near the shallow subduction interface as well as the heterogeneous conditions and deformation caused by seamount subduction. At the Nankai Trough, Yokota et al. (2016) provide the first evidence for the spatial coincidence of low seismic coupling, low-frequency earthquakes, and subducted seamounts on the shallow plate interface derived from seafloor geodetic observations. Their interpretation is that subducting seamounts generate elevated pore fluid pressure and a complicated fracture network that results in low-frequency earthquake activity and reduced coupling. Here we provide additional evidence from seafloor observations at the northern Hikurangi Margin that low-frequency earthquakes are activated in a low-coupled region of the shallow plate interface at a subducting seamount toward the end and following a large slow slip event.

1.1. Northern Hikurangi Slow Slip, Tremor, and Seismicity

New Zealand sits astride the complex boundary between the Australian and Pacific tectonic plates (Figure 1). The Hikurangi Plateau, a large igneous province with a crustal thickness of 10–15 km (Wood & Davy, 1994), subducts beneath the eastern North Island with near trench-perpendicular convergence of ~4.5 cm/year (Wallace et al., 2004) offshore East Cape and strongly oblique convergence offshore Wairarapa, southward to the Chatham Rise. The Hikurangi Margin can be subdivided into three segments: the northern segment, north of Hawke's Bay, the central segment from Hawke's Bay to offshore Wairarapa, and the southern segment between offshore Wairarapa and the end of subduction at the Chatham Rise. We focus on the northern segment of the Hikurangi subduction zone, where the margin is characterized by numerous seamounts on the Hikurangi Plateau and the subduction of these seamounts has played a significant role in the morphology and evolution of the frontal wedge (e.g., Bell et al., 2010; Collot et al., 1996; Pedley et al., 2010). There is an along strike change in the roughness of the incoming Pacific Plate with fewer seamounts emerging above the sedimentary cover in the central and southern segments.

The northern Hikurangi Margin (Figure 1) hosts well-documented shallow recurrent slow slip events as well as associated tectonic tremor and elevated earthquake rates (e.g., Delahaye et al., 2009; Jacobs et al., 2016; Kim et al., 2011; Todd & Schwartz, 2016; Wallace, Beavan, et al., 2012; Wallace & Beavan, 2010). The high density of seismic and cGPS stations along the Raukumara Peninsula closest to the offshore slow slip, the shallow dip of

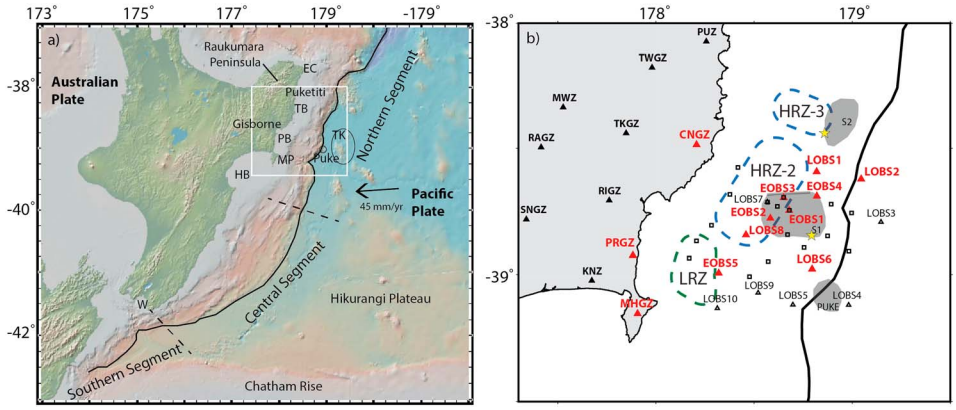

Figure 1. Hikurangi Margin tectonic setting. (a) Topographic/bathymetric relief of the Hikurangi Margin (trench = solid black line) showing a rough incoming Pacific plate in the northern segment with seamounts, the sediment covered central segment, and the obliquely subducting southern segment. Place name abbreviations: W = Wairarapa, HB = Hawke's Bay, MP = Mahia Peninsula, PB = Poverty Bay, TB = Tolaga Bay, EC = East Cape, TK = Tūranganui Knoll. Seamounts Puke and the Tūranganui knoll are circled. The northern Hikurangi Margin study region shown in (b) is identified by the white box. (b) Stations from the offshore Hikurangi Ocean Bottom Investigation of Tremor and Slow Slip (HOBITSS) experiment (triangles = ocean bottom seismometers, squares = absolute pressure gauges) and onshore New Zealand National Seismic Network (triangles = seismometers). Stations in red were used in the detection and location of tectonic tremor. Subducting seamounts S1, S2, and Puke are outlined in gray (Bell et al., 2014). Regions of high-amplitude interface reflectivity (HRZ) and lower amplitude lens reflectivity (LRZ; Bell et al., 2010) are outlined in dashed lines. Epicenters from the 1947 tsunami earthquakes are plotted as yellow stars.

the subducting Hikurangi Plateau, and the resulting shallow depth to the plate interface (12 km near the coast; Eberhart-Phillips & Reyners, 1999; Williams et al., 2013) make the northern Hikurangi Margin an ideal location to investigate the various types of slip behaviors that occur on and near the subduction zone interface. These SSEs, observed since 2002, are primarily short in duration (<20 days), occur at a range of recurrence intervals (<2 years), are equivalent to M_w 6.3–6.8 (Beavan et al., 2007; Douglas et al., 2005; Wallace et al., 2016; Wallace & Beavan, 2010; Wallace, Beavan, et al., 2012), and have most slip located beneath the offshore region.

Tectonic tremor accompanies many northern Hikurangi SSEs, especially those in the Gisborne and Puketiti regions, and has been predominantly located downdip of the geodetically determined slip patches (Kim et al., 2011; Todd & Schwartz, 2016), although tremor collocated with the offshore slow slip is difficult to detect with the land-based New Zealand National Seismic Network. Previously, seismic station density along the Raukumara Peninsula was insufficient to detect and locate tremor associated with offshore SSEs (Delahaye et al., 2009), but beginning in 2010 the seismic station separation was reduced to ~30 km over the entire peninsula and tremor could be detected and located associated with offshore SSEs (Kim et al., 2011; Todd & Schwartz, 2016). In addition to tectonic tremor, the largest SSEs along the northern Hikurangi Margin are also accompanied by increases in seismicity (Delahaye et al., 2009; Jacobs et al., 2016; Todd & Schwartz, 2016), especially with Gisborne and Puketiti SSEs. Although tremor detection is challenging due to highly attenuating sediments beneath the Raukumara Peninsula (Bassett et al., 2014; Eberhart-Phillips & Bannister, 2015; Eberhart-Phillips & Chadwick, 2002; Lewis et al., 1998) and a low seismic station density prior to 2010, it is likely that both tremor and an increase in seismicity accompany many SSEs in the northern Hikurangi Margin.

Two large, M_w 7.2 and 7.1, tsunami earthquakes occurred along the northern segment of the Hikurangi Margin in March and May of 1947, respectively (Bell et al., 2014; Doser & Webb, 2003; Eiby, 1982). Tsunami earthquakes are slow rupturing earthquakes at shallow depths that generate anomalously high tsunami amplitude and runup for their magnitude (Bilek & Lay, 2002; Kanamori, 1972; Pelayo & Wiens, 1992). These tsunami earthquakes occurred in the vicinity of the largest Gisborne SSEs at shallow depths <10 km beneath the continental slope where two seamounts have been subducted and impact the plate interface and the upper plate (seamounts S1 and S2; Figure 1). Although moderate to large interplate earthquakes along the

Hikurangi Margin have been rare in New Zealand's brief historic record, large upper plate and intraslab events such as the 1855 Wairarapa, 1863 and 1931 Hawke's Bay, 2013 Cook Strait sequence, 2016 Te Araroa, and 2016 Kaikoura earthquakes dominate the recent seismic record and demonstrate the complex relationship between upper plate and intraslab faulting and the megathrust.

The geodetic evidence for a largely creeping interface at northern Hikurangi (Wallace et al., 2004) coupled with numerous subducting seamounts suggest that the conceptual model described in Wang and Bilek (2011), whereby subducting seafloor roughness promotes creep could potentially apply to the northern Hikurangi Margin. Subducting seamounts and the resulting complex shear network on the plate interface and in the upper plate could explain the subduction-related strain accumulation and release processes there (see review in Wang & Bilek, 2014). Additionally, subducting seamounts are thought to aid in the subduction of thick fluid-rich sediment packets that become overpressured as they are trapped downdip of the seamount (Bassett et al., 2014; Bell et al., 2010; Ellis et al., 2015). To elucidate the relationship between tremor, earthquakes, and shallow slow slip, and to understand their relative roles and relationship to seamount subduction in northern Hikurangi subduction, we use data from the Hikurangi Ocean Bottom Investigation of Tremor and Slow Slip (HOBITSS) experiment in concert with land-based seismic data to detect and locate tremor and earthquakes during a large SSE offshore Gisborne in 2014. We also compute the changes in Coulomb failure stress imparted on the plate interface by the SSE to estimate the impact these SSEs have in influencing the occurrence and distribution of seismic slip processes on the megathrust.

1.2. Seamount Subduction

Early studies on seamount subduction postulated that topographic relief of the subduction interface increases interplate coupling and provides strongly locked areas that can promote failure in large great subduction earthquakes (e.g., Cloos, 1992; Dmowska et al., 1996; Kelleher & McCann, 1976; Lay et al., 1982). More recent studies of seamount subduction in regional and global contexts have found that seamounts likely break through the upper plate, creating a complex network of fractures and subduct predominantly aseismically (e.g., Bassett & Watts, 2015; von Huene, 2008; Mochizuki et al., 2008; Pedley et al., 2010; Wang & Bilek, 2011, 2014; Yokota et al., 2016). Seamount subduction greatly impacts the evolution and morphology of the Hikurangi Margin (Barker et al., 2009; Collot et al., 1996; Davy & Collot, 2000; Kukowski et al., 2010; Lewis et al., 2004; Lewis & Pettinga, 1993; Pedley et al., 2010). By trapping fluid-rich sediments in front of the seamount in what has been observed on seismic reflection profiles as regions of high-amplitude interface reflectivity (HRZ; Bell et al., 2010) and generating a large, complex fracture network in the upper plate, seamount subduction influences the budget and distribution of fluids on and around the plate interface, and enhances heterogeneity of interface properties. The HRZ can become overpressurized if fluids released during dehydration and compaction are trapped at the downdip edge of the seamount (Ellis et al., 2015). This effect on overpressure is not well understood as the network of complex fractures generated by seamounts breaking through the upper plate (Wang & Bilek, 2014) likely create pathways for fluid migration and the level to which the HRZ can become overpressured is unconstrained. Slow slip is often observed in areas thought to be highly overpressurized regions with low effective stress (e.g., Bassett et al., 2014; Bell et al., 2010; Kitajima & Saffer, 2012; Kodaira et al., 2004) and seamounts predominantly subduct aseismically at shallow depths and may promote weak interplate coupling (e.g., von Huene, 2008; Mochizuki et al., 2008; Wang & Bilek, 2011, 2014) where slow slip is the dominant form of interplate slip.

The presence of numerous seamounts impacting the shallow plate interface of the northern segment of the Hikurangi Margin (Figure 1) coupled with the existence of recorded shallow slow slip along the much of the segment suggest that very rough incoming plates are correlated with the occurrence of shallow episodic slow slip. The northern Hikurangi Margin is established as a region of low interseismic coupling based on GPS measurements (Wallace et al., 2004, 2009). Additionally, the shallow SSEs have been shown to accommodate much of the accumulated strain on the plate interface (Wallace & Beavan, 2010). Between Hawke's Bay and Tolaga Bay (Figure 1), the presence of subducted seamounts likely generates interplate failure in the form of shallow slow slip and promotes the occurrence of tsunami earthquakes. The March (M_w 7.0–7.1) and May (M_w 6.9–7.1) 1947 tsunami earthquakes offshore Gisborne and Tolaga Bay at the edges of seamounts S1 and S2 (Bell et al., 2014) serve as further evidence that the northern margin is weakly coupled and predominantly releases strain through slow slip and tsunami earthquakes.

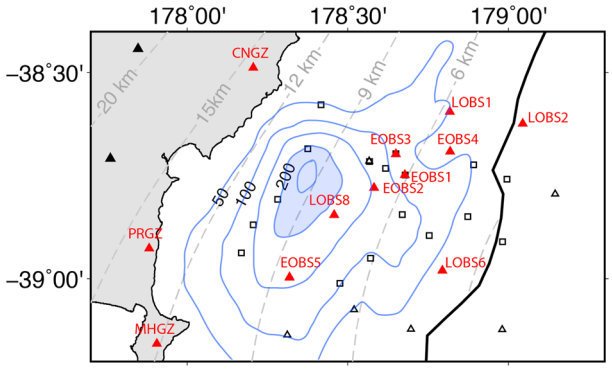

Figure 2. New Zealand National Seismic Network stations (triangles) plotted with ocean bottom seismometers (OBS; triangles) and absolute pressure gauges (APG; squares) from the HOBITSS experiment. The Hikurangi trench (solid black line) and megathrust depth contours (dashed gray lines) are plotted (Williams et al., 2013) with respect to slip contours (solid blue lines; displacement in 50-mm contour intervals) from the 2014 Gisborne SSE (Wallace et al., 2016). The seismic stations with good timing that were used in this study are in red.

2. The HOBITSS Experiment

Since shallow slow slip along the northern Hikurangi is almost entirely offshore, determination of a high-resolution slip distribution is difficult using only terrestrial observations and can be greatly improved with the use of seafloor instrumentation directly above the slip patch (Figure 2). In May 2014, the HOBITSS experiment deployed 24 absolute pressure gauges (APGs) in a near-source array to quantify the extent of seafloor deformation during the SSEs in this region (Wallace et al., 2016). Additionally, 15 ocean bottom seismometers (OBSs) were deployed to detect and locate offshore tectonic tremor and microseismicity and improve the offshore seismic velocity structure. OBS station spacing was densified around a large subducted seamount (seamount S1 in Figure 1b) in order to investigate possible enhanced seismic activity associated with the seamount. By combining slip distributions determined from seafloor geodetic data with seismological data, we clarify the spatiotemporal relationship between slow slip, tremor, and seismicity to improve our understanding of the nature of deformation and stress transfer associated with slow slip. With a well-located offshore earthquake catalog and a well-defined offshore slow slip patch, these data allow for a high-resolution examination of the spatial extent of seismic and aseismic slip.

Nine of the 15 OBS stations recorded data that could be used for detailed, time-sensitive analyses like tremor detection and phase identification used in earthquake location (EOBS 1–5 and LOBS 1, 2, 6, and 8; Figure 2). Unfortunately, two OBS stations did not record seismic data during the slow slip event and four OBS stations had moderate to severe timing errors associated with the seismic data. From the HOBITSS experiment, this study only employs data from the original nine OBS stations without timing errors or data corruption (Figure 2).

A large SSE (equivalent M_w 6.8) occurred in September/October 2014 directly beneath the array and a moderate SSE occurred in December 2014/January 2015 to the south of the array (offshore Mahia Peninsula). Slip from the September/October Gisborne SSE covered an area of approximately 70 by 100 km between 12- and <2-km depth (Figure 2). The peak displacement (>200 mm) was located due east of Poverty Bay at around 9-km depth beneath the continental shelf (Wallace et al., 2016). This study provides a detailed analysis of the spatial and temporal relationships between slow slip, tremor, and earthquakes for the September/October 2014 Gisborne SSE with respect to subducted seamounts using seismic and cGPS data from land stations in the New Zealand National Seismic Network (operated by GeoNet; www.geonet.org.nz) in concert with data from the HOBITSS experiment.

3. Methods

3.1. Tremor Detection and Location

Offshore tectonic tremor is detected and located using the same modified version of the automated envelope cross correlation and grid search methodology described in Todd and Schwartz (2016). Due to increased noise on OBS stations below 3 Hz, the 2–5-Hz band-pass filter used to detect tremor with land stations from the New Zealand National Seismic Network does not adequately isolate tremor energy from background noise or energy from local and regional earthquakes. As a result, envelopes for cross correlation are defined by applying a band-pass filter in two frequency ranges: (1) 4–10 Hz to isolate tremor with energy at lower frequencies and (2) 12–20 Hz to remove local earthquake detections that retain energy above 12 Hz. We analyze the horizontal component of ground motion from four broadband and five short-period ocean bottom seismometers in addition to three land-based coastal seismic stations to increase azimuthal coverage around the geodetically detected slow slip patch for September and October 2014 (Figure 2). Tremor is detected when cross-correlation coefficients on a minimum of seven station pairs exceeds 0.6. When adequate correlations are detected for at least five station pairs in the 12–20-Hz band, the time window is skipped to minimize local earthquake detections. To minimize false detections from regional or teleseismic waves depleted in high-frequency energy, data from a reference station located outside the study region are

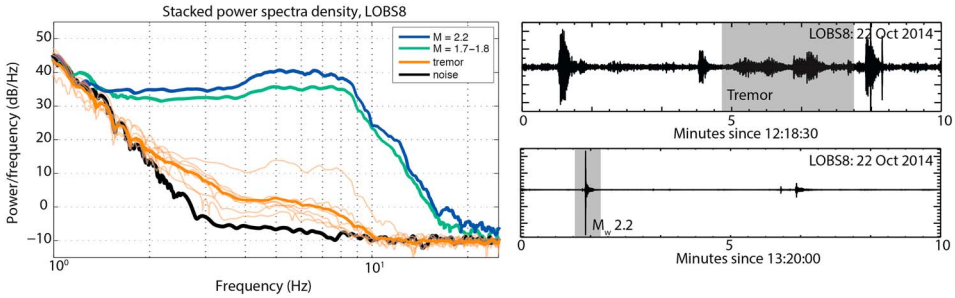

Figure 3. (left) Stacked power spectral densities for earthquakes, tremor (bold orange), and background noise at station LOBS8. Power spectral densities for several individual tremor bursts are shown in light orange. Tremor signals remain above the noise above 2 Hz and fall off rapidly with a corner frequency ~7 Hz, reaching noise levels by 10 Hz. Nearby earthquakes have a higher corner frequency and retain energy above 10 Hz before dropping to noise levels ~25–30 Hz. Noise on OBS drops off between 2 and 3 Hz; therefore, tremor signals have the highest signal to noise at 4–10 Hz. (right) Ten minutes of seismic data from station LOBS8 band-pass filtered at 4–10 Hz with short bursts of tremor (top) and a local M_w 2.2 earthquake (bottom) highlighted in gray. Amplitude scales are scaled to peak amplitudes and differ by 1 order of magnitude between top and bottom plots. Abundant microseismicity and noisy OBS stations make the detection of low-amplitude tremor signals difficult for extended durations. Another example of tremor signal on OBS is down in Figure S1.

filtered from 4–10 Hz and cross correlated with the HOBITSS network. When correlations are detected for at least three station pairs that include the reference station, that time window is removed from further consideration. Though they limit the amount of detected tremor, these steps reduce the number of false tremor detections from the automated process. Once detected, tremor is located by applying the grid search optimization technique described in Wech and Creager (2008) to find centroid locations that minimize *S* wave travel times between the tremor source and correlated station pairs. Since tremor depth is shallow, but poorly constrained, we assume that tremor is located on the plate interface or on thrust faults within the overriding accretionary prism (e.g., Barker et al., 2009; Barnes et al., 2010; Bell et al., 2010). Tremor event details are presented in Table S1.

To ensure that the tremor signal is distinct from local microearthquakes, we compare the spectral characteristics of the tremor signal to that of nearby earthquakes. The power spectral densities for 56 ten-second time windows of tremor are compared to background noise and nearby earthquakes thought to be on the plate interface at station LOBS8 (Figure 3). These earthquakes are distinguished from tremor because they retain high-frequency energy above 10 Hz while tremor is indistinguishable from noise above 10 Hz. Additionally, background noise on OBS stations remains high until 2–3 Hz, so tremor signals are most apparent between 4–10 Hz.

3.2. Detecting and Locating Local Earthquakes

Earthquakes were manually detected for September and October 2014 by picking *P* wave arrivals at up to nine OBS stations and 16 land seismic stations for over 850 visually identified events (Table S2). Using a local 1-D interpretation of the New Zealand 3-D velocity model (Eberhart-Phillips et al., 2010; Reyners et al., 1999), preliminary hypocenters for over 600 events were found using Antelope's *dblocsat2* algorithm that minimizes travel times over a 3-D grid search. Hypocentral locations were improved by relocating events with NonLinLoc v.6.0, a probabilistic nonlinear relocation program that calculates the maximum likelihood hypocenter within a probability density function through a 3-D grid search (Lomax et al., 2000). Horizontal location errors as indicated by the probability density function are typically on the order of a few kilometers ($<$10 km). Emphasis was placed on events located near the slow slip displacement shown in Figure 2.

3.3. Calculating Changes in Coulomb Failure Stress

To establish the effects of slow slip on the stress state of the surrounding plate boundary, we employ the most recently published geometry of the Hikurangi subduction interface (Williams et al., 2013) and PyLith, a finite element crustal deformation modeling tool (Aagaard et al., 2013, 2016), to compute Coulomb failure stress changes on the plate interface utilizing both normal and shear stress changes. We use the slow slip distribution determined by Wallace et al. (2016) using horizontal and vertical displacements from onshore GPS sites, and vertical displacements from seafloor absolute pressure gauge data collected during the HOBITSS

experiment. The slip distribution with a slip cutoff value of 1 mm is transferred from the coarse grid used in the geodetic inversion to the Hikurangi megathrust geometry and projected onto a finer-scale mesh using bilinear interpolation and then smoothed to mitigate the effects of stress singularities due to gradients in the original slip distribution. PyLith is then used to compute the traction changes for each element in the fault mesh. We determine the change in Coulomb failure stress from the computed fault-normal stresses and map the computed shear traction changes onto the direction of plate convergence (Wallace, Barnes, et al., 2012) for each element in the mesh to calculate the shear stresses. We then use these stresses and a constant apparent coefficient of friction of 0.4 to compute the change in Coulomb failure stress imparted on the megathrust during the 2014 SSE.

4. Results and Discussion

4.1. Tremor Collocated With Slow Slip and Subducted Seamounts

Prior to the HOBITSS experiment, tremor could only be detected with seismic data from land stations after the network achieved sufficient density in 2010. For the Gisborne SSEs, these detections are temporally correlated with the SSEs and are predominantly located onshore in bands that extend west and northwest from the downdip edge of geodetically detected slow slip (Figure 4). While northern Hikurangi tremor beneath the land is temporally coincident with offshore SSEs (Kim et al., 2011; Todd & Schwartz, 2016), offshore tremor spatially collocated with slow slip has not been previously observed. This is unlike most other tremorgenic subduction zones such as Cascadia or Nankai where tremor occurring during slow slip is identified to be predominantly collocated with the slow slip patch (e.g., Ghosh et al., 2009; Ito et al., 2007). The slow slip with collocated tremor in these regions is located significantly deeper (30–50 km) than slow slip along the northern Hikurangi Margin ($<$12 km); at this depth, the slow slip and tremor sit directly beneath landmasses that can be well instrumented for real-time monitoring, thus making tremor detection easier and more robust. By instrumenting the seafloor directly above Gisborne slow slip, the HOBITSS experiment provides an opportunity to observe tremor within a shallow, offshore slow slip patch.

Offshore tremor associated with the 2014 Gisborne SSE is clustered updip of the northern end of the geodetically detected peak (200+ mm) slip (Wallace et al., 2016) atop and around the downdip edge of a large subducted seamount (seamount S1; Figure 4). This cluster of tremor events updip of the peak slow slip forms an offshore extension of previously detected tremor activity associated with the 2014 Gisborne SSE (dark gray circles; Figure 4) that extends onshore and downdip from the slow slip patch. Tremor has been detected in the same onshore region, downdip of the slow slip patch for every Gisborne SSE since 2010 (Todd & Schwartz, 2016). Here we present the first observation of offshore tremor that is collocated with geodetically detected slow slip along the northern Hikurangi Margin.

Wallace et al. (2016) show that APGs across the HOBITSS network experience upward movement of the ocean floor beginning on Julian days (JD) 262–265 and continuing for two to three weeks. This time period corresponds with a small shallow episode of tremor south of station LOBS6 near the trench where seamount Puke is currently subducting (Figure 4). After infrequent tremor for the first 10–15 days of slow slip, a burst of tremor activity begins between JD 275–277, again focused at the Puke seamount. Although tremor detection is most robust in areas of high seismic station density near seamount S1, the location of abundant tremor in the southeast quadrant, near Puke seamount, indicates that the HOBITSS network combined with three coastal seismic stations provides sufficient density to detect and locate tremor within the entire network. Toward the end of the upward motion detected on the APG, a second, longer episode of tremor begins near station LOBS8 on JD 279 and continues across the leading edge of subducted seamount S1 toward station LOBS1 in a northwest trend through the end of the month (JD 304). While the observable upward motion on the APGs tapers off around JD 283–290, tremor activity continues to move northeastward across the seamount for an additional two to three weeks. If this episode of tremor corresponds with a slowly moving slow slip front with seafloor deformation below the APG detection threshold, the slow slip duration may be longer than previously thought. The delayed onset of updip tremor with respect to the geodetically determined slow slip differs from the downdip Gisborne tremor (Kim et al., 2011; Todd & Schwartz, 2016) and from most observations in other subduction zones (e.g., Wech et al., 2009) where tremor and measurable slow slip are temporally coincident. The large northeastward migrating tremor episode corresponds to a velocity of ~0.7 km/day (Figure 4), a considerably lower velocity than tremor migration observed in Cascadia and

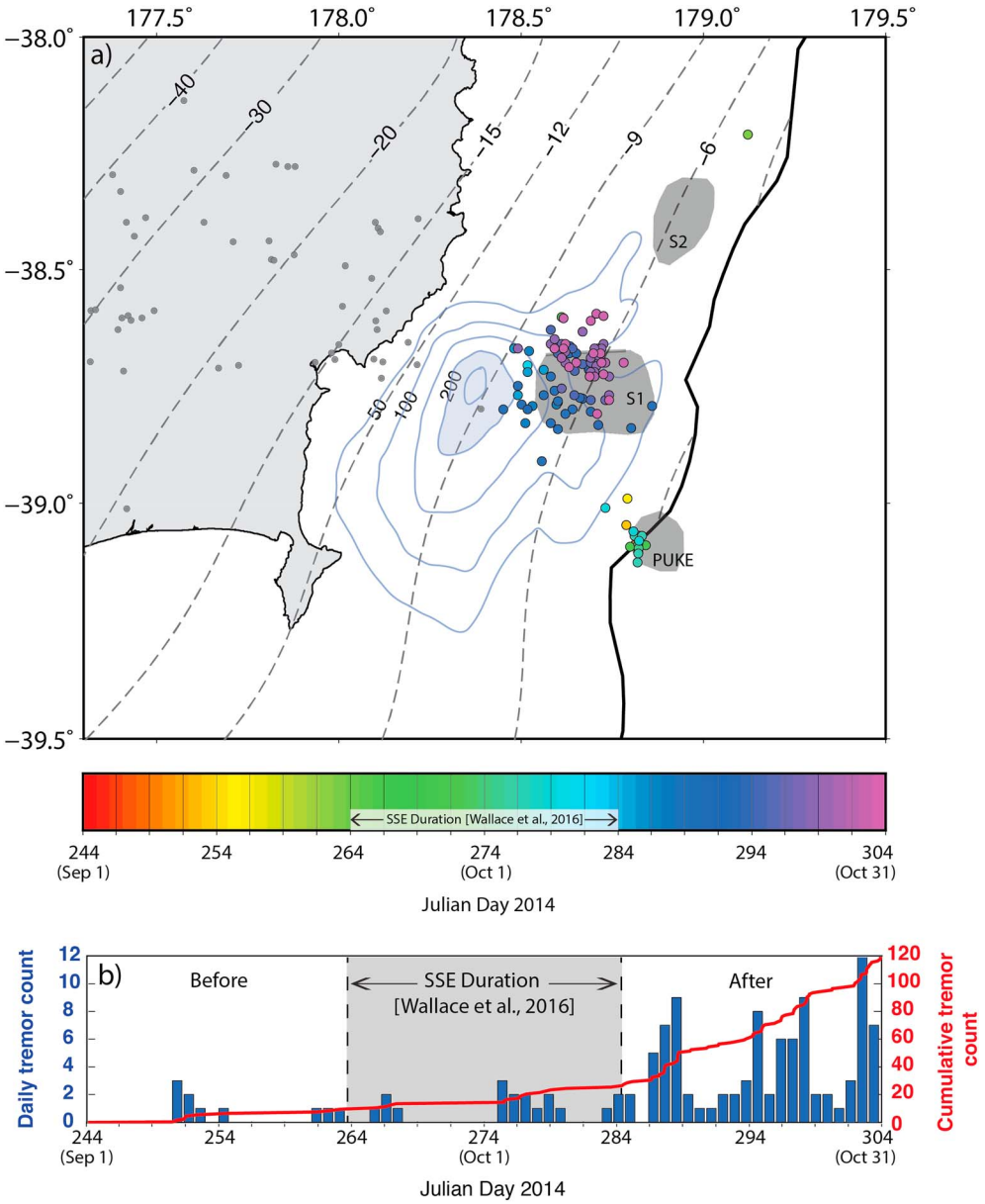

Figure 4. (a) Tectonic tremor associated with the 2014 Gisborne SSE. Offshore tremor (circles color coded by time) is primarily located on and downdip of the estimated location of subducted seamount S1 from Bell et al. (2014), updip of the peak displacement in the slip event. Onshore tremor events located with land-based stations in the New Zealand National Seismic Network from Todd and Schwartz (2016) (dark gray circles) are located downdip of the peak slip extending in the dip direction. We assume that tremor is located on the plate interface or on accretionary prism thrusts in the upper plate. (b) Daily tremor count for September and October 2014 (JD 244–304) in blue and cumulative earthquake count in red. The tremor rate begins to change in the middle of the geodetically detected slow slip (~JD 274) and changes significantly after the final days of the SSE (~JD 287).

Nankai with velocities of 5–15 km/day (Ide, 2010; Kao et al., 2006; McCausland et al., 2010; Obara & Sekine, 2009). This slow tremor migration velocity may be due to the shallow depth of the slip. Assuming the tremor is located on or near the plate interface, this tremor migration occurs along strike between 3- and 9-km depth, beneath the accretionary wedge.

Both identifiable bursts of offshore tremor activity occur in the vicinity of the subducted seamounts Puke and S1 (Figure 4), suggesting that a complicated network of shear fractures expected to surround the subducted seamounts may influence tremorgenesis in the northern segment of the Hikurangi Margin. Although

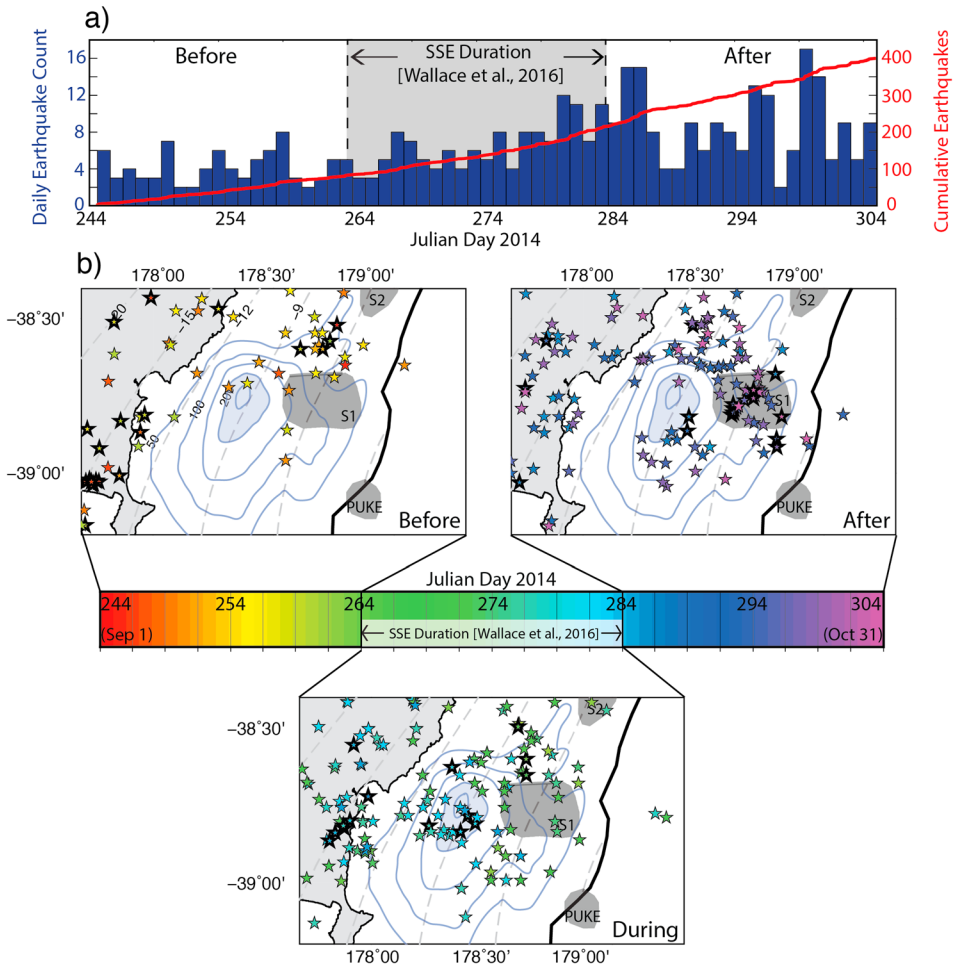

Figure 5. (a) Earthquakes (stars, color coded with time) before, during, and after geodetically detected slow slip with respect to subducted seamounts and slow slip displacement. Events with bold outlines are located within 5 km of the plate interface. Earthquakes are located in the region of peak slip at the start of the SSE and are concentrated on the north edge of the slip patch after the SSE. (b) Daily earthquake count for September and October 2014 (JD 244–304) in blue and cumulative earthquake count in red. The earthquake rate changes once the slow slip begins (~JD 264) and increases more in the final days of the SSE around JD 278.

seamounts are suggested by some to primarily subduct aseismically (Mochizuki et al., 2008; Wang & Bilek, 2014), tectonic tremor, assumed to be located on the plate interface or on thrust faults within the accretionary prism, that is strongly spatially correlated with slow slip and seamounts may be a seismic manifestation of seamount subduction. Additionally, the complex fracture pattern generated by the "breaking through" method of seamount subduction (Dominguez et al., 1998; Ruh et al., 2016; Wang & Bilek, 2011, 2014) creates numerous connected fluid pathways that could promote low-magnitude slow slip across the seamount.

4.2. Seismicity Before, During, and After Slow Slip

Clear seismicity increases do not accompany every shallow SSE along the northern Hikurangi Margin, but significant increases have been identified during the largest shallow SSEs such as the 2004 and 2010 Gisborne SSEs, and the 2011 Cape Turnagain SSE (Bartlow et al., 2014; Delahaye et al., 2009; Jacobs et al., 2016; Wallace, Beavan, et al., 2012). The 2014 Gisborne SSE has a small increase in seismicity starting at the beginning of the geodetically detected slip that continues for several days with the largest increase in seismicity rate occurring toward the end of the slip event. Focusing on earthquakes located near the shoreline and offshore provides a detailed look at where earthquakes are occurring before, during, and after the 2014 Gisborne SSE (Figure 5). For the purposes of this discussion, earthquakes that locate within 5-km depth of the plate interface

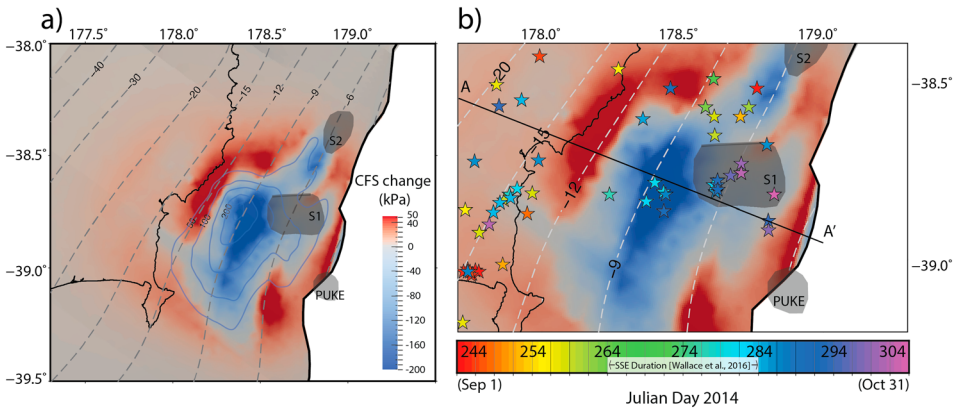

Figure 6. (a) Calculations of the Coulomb failure stress change (CFS) imparted on the megathrust by the 2014 Gisborne SSE. Regions of stress increase are shown in red and regions of stress decrease are shown in blue. (b) Earthquakes (stars, color coded with time) located within 5 km of the plate interface (and assumed to be on the plate interface for the purposes of this discussion) are plotted with the CFS change and seamounts Puke, S1, and S2. Stress changes from the SSE do not appear to greatly impact interplate faulting. Depths of earthquakes along transect A-A′ are plotted in Figure S2.

determined by Williams et al. (2013) are considered to be interplate earthquakes (Figure S2). Interplate earthquakes detected before the SSE are primarily located onshore between Poverty Bay and the Mahia Peninsula or offshore, north of seamount S1, and downdip from seamount S2 in the region that will slip in the event between 6- and 9-km depth. Once the SSE begins, earthquakes continue at the updip edge of the slip, adjacent to seamount S1 until ~JD 279 when several earthquakes occur on the plate interface (within 5 km) in the vicinity of the peak displacement (>200 mm) from the slow slip. The presence of interplate earthquakes in the northern finger of the slip patch, prior to the geodetically determined onset of slow slip, followed by earthquakes in close proximity to the peak displacement suggests that slow slip may have initiated in the north, downdip of seamount S2 as early as JD 252 before advancing southward along strike. After the end of geodetically detected slow slip, earthquake activity in the peak slow slip patch ceases and seismicity clusters near seamount S1 (Figure 5) very similar to the tremor behavior (Figure S3). These events are too small to determine focal mechanisms for, but are limited to be within 5-km depth of the plate interface and may be located in the fractures above the seamount. Since the slow slip is offshore, small offshore earthquake sequences may accompany all Gisborne SSEs, but are difficult to detect with the land-based seismic network.

4.3. Change in Coulomb Failure Stress on Megathrust From Slow Slip

The relationship between the distribution of aftershocks and the static increase in Coulomb failure stress (CFS) has been well established (e.g., Stein, 1999; Stein et al., 1992; Stein & Lisowski, 1983; Toda et al., 1998). Additionally, earthquakes, tectonic tremor, and slow slip events can be dynamically triggered by the passage of seismic waves from regional and teleseismic earthquakes (e.g., Chao et al., 2013; Fry et al., 2011; Hill et al., 1993; Peng et al., 2009; Prejean et al., 2004; Wallace et al., 2017; Zigone et al., 2012). To further investigate the relationship between slow slip, tremor, and earthquakes on or near the plate interface we compute the change in CFS on the plate interface and look at the regions of stress increase with respect to the tremor and earthquake distribution during and after the 2014 Gisborne SSE. Tectonic tremor predominantly occurs near the end and continues after the geodetically observed slow slip event. The temporal delay in the occurrence of tremor may be triggered by stress changes induced by the slow slip. Results from our CFS calculations are shown in Figure 6 where most of the slow slip region experiences a decrease of >30 kPa (peak ~180 kPa). The only part of the slow slip patch that does not experience a stress decrease >30 kPa is where seamount S1 is located. Slip inversions with land stations and the APG data predict less displacement (<100 mm) across the seamount (Wallace et al., 2016), and this is reflected in the CFS calculations as the peak stress decrease wraps around the seamount's downdip edge. Downdip of the peak slip and seamount S1, the plate interface experiences an increase in CFS of >30 kPa with a peak of around 50 kPa in a region where tremor associated with SSEs has been previously observed (Kim et al., 2011; Todd & Schwartz, 2016). A CFS increase is also experienced updip of the southern part of the slow slip patch with an increase of >30 kPa.

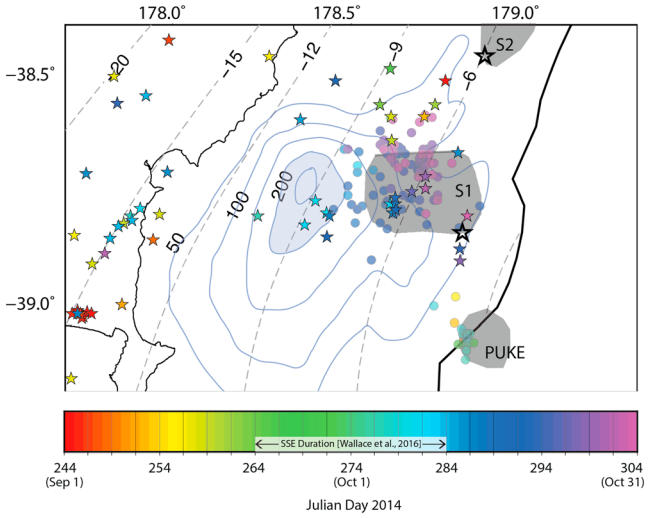

Figure 7. Various modes of slip on the plate interface (depth contours are dashed gray lines; labeled in km) are plotted together with the subducted seamounts Puke, S1, and S2 (Bell et al., 2014). Slow slip displacement (blue contours; displacement in mm), tectonic tremor (circles), and interplate earthquakes (stars). The 1947 tsunami earthquake epicenters plotted as open black stars.

These values of CFS increase are similar to the increases computed for regular earthquakes similar in magnitude to the 2014 Gisborne SSE (equivalent M_w 6.7–6.8). For example, the 2002 M_w 6.7 Nenana Mountain earthquake, a foreshock to the M_w 7.9 Denali earthquake, generated a CFS increase of 30–50 kPa in the hypocentral region of the main shock (Anderson & Ji, 2003).

Earthquakes within 5 km of the plate interface are plotted with the CFS change calculations in Figure 6b and are considered to be on the plate interface for the purposes of this study (Figures S2 and S3). These earthquakes are clustered at the northern edge of the slow slip patch, within and immediately north of seamount S1. Earthquakes within the slow slip patch begin around JD 278–284 in the region that experiences the greatest displacement (>150 mm) and the greatest decrease in CFS in the final days of the geodetically detected slip event. Since the slip distribution of the SSE is applied as an instantaneous event, we cannot see the time evolution of the slip and stress changes. Time-dependent slip inversions are needed to obtain a higher-resolution view of the change in CFS with time. During the same time period, earthquakes occur downdip of the slow slip patch along the coast between Poverty Bay and the Mahia Peninsula as well as along the northern coast of Hawke's Bay. Interestingly, there is no clear concentration of earthquakes on the megathrust in the regions experiencing the largest increase in CFS. Rather, many of the event locations appear to be unrelated to the CFS increases. The same is true of the tremor, since tremor clustered near seamount S1, similar to the interplate earthquake locations. With the majority of earthquakes and tremor occurring near seamount S1 and Puke seamount, it appears as though the subduction of these seamounts dominates the stress field and plays a large role in the localization of interplate seismicity. Of course, unmodeled details and complexities in the slow slip distribution and the geometry of the subduction interface can have a large affect on the resulting CFS calculations.

4.4. Slip Heterogeneity on the Shallow Megathrust

Figure 7 illustrates the location of the diverse modes of interplate slip associated with the 2014 Gisborne SSE. Each unique mode, (1) fast, regular earthquakes; (2) tremor; (3) tsunami earthquakes (such as the 1947 events); and (4) large, geodetically detected slow slip, are largely interspersed together. While the majority of the shallow plate interface at the northern Hikurangi Margin slips too slowly to radiate seismic energy, some small patches, clustered near seamounts, slip fast enough to generate tremor while larger patches are able to nucleate microseismicity and even tsunami earthquakes (e.g., 1947 events). This observation supports a model where seamount subduction produces a heterogeneous stress state, a complex fracture system, and pore fluid pressure conditions capable of hosting a wide range of transient events with varied magnitudes and slip rates in close proximity. Similar observations have been made offshore central Ecuador where seismic imaging of subducted oceanic relief together with GPS data from coastal and island sites resolve heterogeneous shallow plate coupling consisting of locked patches, frequent slow slip events, and repeating earthquake swarms (Collot et al., 2017; Vallée et al., 2013). Collot et al. (2017) speculate that stress increases due to slow slip events generate seismic rupture on secondary faults close to failure within the subducted seafloor relief. We invoke a similar process to explain the close association of earthquakes and tremor with subducted seamounts in the Hikurangi subduction zone. Further analysis of these events is warranted to determine if they are on the plate interface, in the fractured upper plate above the seamount, or in the subducted plate. The tsunami earthquake of March 1947 also originated near seamount S1 and may have ruptured across the seamount (Bell et al., 2014), further suggesting that this seamount may be influencing the stress state and mechanisms of interplate slip.

5. Conclusions

One primary goal of the HOBITSS experiment was to determine if slow and fast interplate slip modes (i.e., slow slip, tremor, and microseismicity) spatially overlap or were segregated. The northern segment of the

Hikurangi Margin experiences seamount subduction that produces a heterogeneous environment that hosts a range of interfingered interplate slip processes. Using data from the HOBITSS experiment, we find that tremor is not only temporally correlated with slow slip as it occurs onshore, downdip of the slip patch, but is collocated with slow slip offshore. We detect two distinct tremor episodes that strongly overlap in space with the locations of two shallowly (<6 km) subducted seamounts. The second of these tremor episodes shows a slow northeast migration across the downdip edge of seamount S1 that persists for a couple of weeks after the geodetically detected SSE ends. Subduction of northern Hikurangi seamounts may generate elevated pore fluid pressures at the leading edge of the seamount in accumulated underplated sediment packages and a complex, interconnected fracture network such that during shallow slow slip, tremor and microseismicity may join tsunami earthquakes as a seismic component of subduction. This occurrence of tremor with subducted seamounts supports the findings of Yokota et al. (2016) that subducting seamounts generate elevated pore fluid pressure that can result in low-frequency earthquake activity. CFS change calculations show stress increases at the updip and downdip edges of the slow slip patch that have a complex relationship with the distribution of interplate earthquakes. This detailed investigation into the 2014 Gisborne SSE indicates that the location of subducted seamounts strongly correlates with the distribution of SSE-associated tectonic tremor and shows that the seamounts may experience slow slip, tremor, microseismicity, and large tsunami earthquakes, rupturing the same portions of the plate interface in a range of slip processes.

Acknowledgments

We acknowledge support from U.S. NSF grant IIA-1414769 to E.K.T. as part of the East Asia and Pacific Summer Institute; OCE-1334654, 1333311, 1332875, and 1333025 to L.M.W., S.C.W., S.Y.S., and A. F.S.; and Japan Society for the Promotion of Science grant KAKENHI-26257206 to Y.I. and KAKENHI JP16H06415 to K.M. Raw data from the experiment are archived at the Incorporated Research Institutions for Seismology Data Management Center (DOI: https://doi.org/10.7914/SN/YH_2014). Additional funding support came from Japan's Ministry of Education, Culture, Sports, Science, and Technology; the Earthquake Research Institute; the University of Tokyo Joint Usage/Research Program; and the International Research Institute of Disaster Science at Tohoku University. Support for ship time was provided by NSF, GNS Science, and Land Information New Zealand's Oceans 2020 program. We greatly appreciate the immense contribution to the success of this project from ocean bottom instrument engineering teams at LDEO, UTIG, University of Tokyo, and Tohoku University, as well as the captain and crew of the U.S. R/V *Roger Revelle* and New Zealand R/V *Tangaroa*. Seismic data from the New Zealand National Seismic Network are available from GeoNet (http://geonet.org.nz). Data required to reach the conclusions presented in this paper that are not contained within it, its references, and/or the supporting information may be requested from the authors.

References

Aagaard, B. T., Knepley, M. G., & Williams, C. A. (2013). A domain decomposition approach to implementing fault slip in finite-element models of quasi-static and dynamic crustal deformation. *Journal of Geophysical Research: Solid Earth*, *118*, 3059–3079. https://doi.org/10.1002/jgrb.50217

Aagaard, B. T., Knepley, M. G., & Williams, C. A. (2016). *PyLith User Manual, Version 2.1.4.* . Davis, CA: Computational Infrastructure of Geodynamics. Retrieved from https://geodynamics.org/cig/software/github/pylith/v2.1.4/pylith-2.1.4_manual.pdf

Anderson, G., & Ji, C. (2003). Static stress transfer during the 2002 Nenana Mountain-Denali Fault, Alaska, earthquake sequence. *Geophysical Research Letters*, *30*(6), 1310. https://doi.org/10.1029/2002GL016724

Barker, D. H. N., Sutherland, R., Henrys, S., & Bannister, S. (2009). Geometry of the Hikurangi subduction thrust and upper plate, North Island, New Zealand. *Geochemistry, Geophysics, Geosystems*, *10*, Q02007. https://doi.org/10.1029/2008GC002153

Barnes, P. M., Lamarche, G., Bialas, J., Henrys, S., Pecher, I., Netzeband, G. L., et al. (2010). Tectonic and geological framework for gas hydrates and cold seeps on the Hikurangi subduction margin, New Zealand. *Marine Geology*, *272*(1), 26–48. https://doi.org/10.1016/j.margeo.2009.03.012

Bartlow, N. M., Wallace, L. M., Beavan, R. J., Bannister, S., & Segall, P. (2014). Time-dependent modeling of slow slip events and associated seismicity and tremor at the Hikurangi subduction zone, New Zealand. *Journal of Geophysical Research: Solid Earth*, *119*, 734–753. https://doi.org/10.1002/2013JB010609

Bassett, D., Sutherland, R., & Henrys, S. (2014). Slow wavespeeds and fluid overpressure in a region of shallow geodetic locking and slow slip, Hikurangi subduction margin, New Zealand. *Earth and Planetary Science Letters*, *389*, 1–13. https://doi.org/10.1016/j.epsl.2013.12.021

Bassett, D., & Watts, A. B. (2015). Gravity anomalies, crustal structure, and seismicity at subduction zones: 1. Seafloor roughness and subducting relief. *Geochemistry, Geophysics, Geosystems*, *16*, 1508–1540. https://doi.org/10.1002/2014GC005684

Beavan, J., Wallace, L. M., Fletcher, H., & Douglas, A. (2007). Slow slip events on the Hikurangi subduction interface, New Zealand. In D. P. Tregoning & D. C. Rizos (Eds.), *Dynamic Planet* (pp. 438–444). Berlin, Heidelberg: Springer. https://doi.org/10.1007/978-3-540-49350-1_64

Bell, R., Holden, C., Power, W., Wang, X., & Downes, G. (2014). Hikurangi margin tsunami earthquake generated by slow seismic rupture over a subducted seamount. *Earth and Planetary Science Letters*, *397*, 1–9. https://doi.org/10.1016/j.epsl.2014.04.005

Bell, R., Sutherland, R., Barker, D. H. N., Henrys, S., Bannister, S., Wallace, L. M., & Beavan, J. (2010). Seismic reflection character of the Hikurangi subduction interface, New Zealand, in the region of repeated Gisborne slow slip events. *Geophysical Journal International*, *180*(1), 34–48. https://doi.org/10.1111/j.1365-246X.2009.04401.x

Beroza, G. C., & Ide, S. (2011). Slow earthquakes and nonvolcanic tremor. *Annual Review of Earth and Planetary Sciences*, *39*(1), 271–296. https://doi.org/10.1146/annurev-earth-040809-152531

Bilek, S. L., & Lay, T. (2002). Tsunami earthquakes possibly widespread manifestations of frictional conditional stability. *Geophysical Research Letters*, *29*(14), 1673. https://doi.org/10.1029/2002GL015215

Chao, K., Peng, Z., Gonzalez-Huizar, H., Aiken, C., Enescu, B., Kao, H., et al. (2013). A Global Search for Triggered Tremor Following the 2011 M_w 9.0 Tohoku earthquake. *Bulletin of the Seismological Society of America*, *103*(2B), 1551–1571. https://doi.org/10.1785/0120120171

Cloos, M. (1992). Thrust-type subduction-zone earthquakes and seamount asperities: A physical model for seismic rupture. *Geology*, *20*(7), 601–604. https://doi.org/10.1130/0091-7613(1992)020<0601:TTSZEA>2.3.CO;2

Collot, J.-Y., Delteil, J., Lewis, K. B., Davy, B., Lamarche, G., Audru, J.-C., et al. (1996). From oblique subduction to intra-continental transpression: Structures of the southern Kermadec-Hikurangi margin from multibeam bathymetry, side-scan sonar and seismic reflection. *Marine Geophysical Researches*, *18*(2–4), 357–381. https://doi.org/10.1007/BF00286085

Collot, J. -Y., Sanclemente, E., Nocquet, J.-M., Angélique, L., Alessandra, R., Paul, J., et al. (2017). Subducted oceanic relief locks the shallow megathrust in central Ecuador. *Journal of Geophysical Research: Solid Earth*, *122*, 3286–3305. https://doi.org/10.1002/2016JB013849

Davy, B., & Collot, J.-Y. (2000). The Rapuhia Scarp (northern Hikurangi Plateau)—Its nature and subduction effects on the Kermadec Trench. *Tectonophysics*, *328*(3–4), 269–295. https://doi.org/10.1016/S0040-1951(00)00211-0

Delahaye, E. J., Townend, J., Reyners, M. E., & Rogers, G. (2009). Microseismicity but no tremor accompanying slow slip in the Hikurangi subduction zone, New Zealand. *Earth and Planetary Science Letters*, *277*(1–2), 21–28. https://doi.org/10.1016/j.epsl.2008.09.038

Dmowska, R., Zheng, G., & Rice, J. R. (1996). Seismicity and deformation at convergent margins due to heterogeneous coupling. *Journal of Geophysical Research*, *101*(B2), 3015–3029. https://doi.org/10.1029/95JB03122

Dominguez, S., Lallemand, S. E., Malavieille, J., & von Huene, R. (1998). Upper plate deformation associated with seamount subduction. *Tectonophysics*, *293*(3–4), 207–224. https://doi.org/10.1016/S0040-1951(98)00086-9

Doser, D. I., & Webb, T. H. (2003). Source parameters of large historical (1917–1961) earthquakes, North Island, New Zealand. *Geophysical Journal International*, *152*(3), 795–832. https://doi.org/10.1046/j.1365-246X.2003.01895.x

Douglas, A., Beavan, J., Wallace, L. M., & Townend, J. (2005). Slow slip on the northern Hikurangi subduction interface, New Zealand. *Geophysical Research Letters*, *32*, L16305. https://doi.org/10.1029/2005GL023607

Dragert, H., Wang, K., & James, T. S. (2001). A silent slip event on the deeper Cascadia subduction interface. *Science*, *292*(5521), 1525–1528. https://doi.org/10.1126/science.1060152

Eberhart-Phillips, D., & Bannister, S. (2015). 3-D imaging of the northern Hikurangi subduction zone, New Zealand: Variations in subducted sediment, slab fluids and slow slip. *Geophysical Journal International*, *201*(2), 838–855. https://doi.org/10.1093/gji/ggv057

Eberhart-Phillips, D., & Chadwick, M. (2002). Three-dimensional attenuation model of the shallow Hikurangi subduction zone in the Raukumara Peninsula, New Zealand. *Journal of Geophysical Research*, *107*(B2), 2033. https://doi.org/10.1029/2000JB000046

Eberhart-Phillips, D., & Reyners, M. (1999). Plate interface properties in the Northeast Hikurangi Subduction Zone, New Zealand, from converted seismic waves. *Geophysical Research Letters*, *26*(16), 2565–2568. https://doi.org/10.1029/1999GL900567

Eberhart-Phillips, D., Reyners, M., Bannister, S., Chadwick, M., & Ellis, S. (2010). Establishing a versatile 3-D seismic velocity model for New Zealand. *Seismological Research Letters*, *81*(6), 992–1000. https://doi.org/10.1785/gssrl.81.6.992

Eiby, G. A. (1982). Two New Zealand tsunamis. *Journal of the Royal Society of New Zealand*, *12*(4), 338–351. https://doi.org/10.1080/03036758.1982.10415340

Ellis, S., Fagereng, Å., Barker, D., Henrys, S., Saffer, D., Wallace, L. M., et al. (2015). Fluid budgets along the northern Hikurangi subduction margin, New Zealand: The effect of a subducting seamount on fluid pressure. *Geophysical Journal International*, *202*(1), 277–297. https://doi.org/10.1093/gji/ggv127

Fry, B., Chao, K., Bannister, S., Peng, Z., & Wallace, L. M. (2011). Deep tremor in New Zealand triggered by the 2010 M_w8.8 Chile earthquake. *Geophysical Research Letters*, *38*, L15306. https://doi.org/10.1029/2011GL048319

Ghosh, A., Vidale, J. E., Sweet, J. R., Creager, K. C., & Wech, A. G. (2009). Tremor patches in Cascadia revealed by seismic array analysis. *Geophysical Research Letters*, *36*, L17316. https://doi.org/10.1029/2009GL039080

Hill, D. P., Reasenberg, P. A., Michael, A., Arabaz, W. J., Beroza, G., Brumbaugh, D., et al. (1993). Seismicity remotely triggered by the magnitude 7.3 Landers, California, earthquake. *Science*, *260*(5114), 1617–1623.

Hirose, H., Hirahara, K., Kimata, F., Fujii, N., & Miyazaki, S. (1999). A slow thrust slip event following the two 1996 Hyuganada earthquakes beneath the Bungo Channel, southwest Japan. *Geophysical Research Letters*, *26*(21), 3237–3240. https://doi.org/10.1029/1999GL010999

Hirose, H., & Obara, K. (2005). Repeating short- and long-term slow slip events with deep tremor activity around the Bungo channel region, southwest Japan. *Earth, Planets and Space*, *57*(10), 961–972. https://doi.org/10.1186/BF03351875

Ide, S. (2010). Striations, duration, migration and tidal response in deep tremor. *Nature*, *466*(7304), 356–359. https://doi.org/10.1038/nature09251

Ito, Y., Obara, K., Shiomi, K., Sekine, S., & Hirose, H. (2007). Slow earthquakes coincident with episodic tremors and slow slip events. *Science*, *315*(5811), 503–506. https://doi.org/10.1126/science.1134454

Jacobs, K. M., Savage, M. K., & Smith, E. C. G. (2016). Quantifying seismicity associated with slow slip events in the Hikurangi margin, New Zealand. *New Zealand Journal of Geology and Geophysics*, *59*(1), 58–69. https://doi.org/10.1080/00288306.2015.1127827

Jiang, Y., Wdowinski, S., Dixon, T. H., Hackl, M., Protti, M., & Gonzalez, V. (2012). Slow slip events in Costa Rica detected by continuous GPS observations, 2002–2011. *Geochemistry, Geophysics, Geosystems*, *13*, Q04006. https://doi.org/10.1029/2012GC004058

Kanamori, H. (1972). Mechanism of tsunami earthquakes. *Physics of the Earth and Planetary Interiors*, *6*(5), 346–359. https://doi.org/10.1016/0031-9201(72)90058-1

Kao, H., Shan, S.-J., Dragert, H., Rogers, G., Cassidy, J. F., Wang, K., et al. (2006). Spatial-temporal patterns of seismic tremors in northern Cascadia. *Journal of Geophysical Research*, *111*, B03309. https://doi.org/10.1029/2005JB003727

Kaproth, B. M., & Marone, C. (2013). Slow earthquakes, preseismic velocity changes, and the origin of slow frictional stick-slip. *Science*, *341*(6151), 1229–1232. https://doi.org/10.1126/science.1239577

Kelleher, J., & McCann, W. (1976). Buoyant zones, great earthquakes, and unstable boundaries of subduction. *Journal of Geophysical Research*, *81*(26), 4885–4896. https://doi.org/10.1029/JB081i026p04885

Kim, M. J., Schwartz, S. Y., & Bannister, S. (2011). Non-volcanic tremor associated with the March 2010 Gisborne slow slip event at the Hikurangi subduction margin, New Zealand. *Geophysical Research Letters*, *38*, L14301. https://doi.org/10.1029/2011GL048400

Kitajima, H., & Saffer, D. M. (2012). Elevated pore pressure and anomalously low stress in regions of low frequency earthquakes along the Nankai Trough subduction megathrust. *Geophysical Research Letters*, *39*, L23301. https://doi.org/10.1029/2012GL053793

Kodaira, S., Iidaka, T., Kato, A., Park, J.-O., Iwasaki, T., & Kaneda, Y. (2004). High pore fluid pressure may cause silent slip in the Nankai Trough. *Science*, *304*(5675), 1295–1298. https://doi.org/10.1126/science.1096535

Kostoglodov, V., Singh, S. K., Santiago, J. A., Franco, S. I., Larson, K. M., Lowry, A. R., & Bilham, R. (2003). A large silent earthquake in the Guerrero seismic gap, Mexico. *Geophysical Research Letters*, *30*(15), 1807. https://doi.org/10.1029/2003GL017219

Kukowski, N., Greinert, J., & Henrys, S. (2010). Morphometric and critical taper analysis of the Rock Garden region, Hikurangi Margin, New Zealand: Implications for slope stability and potential tsunami generation. *Marine Geology*, *272*(1–4), 141–153. https://doi.org/10.1016/j.margeo.2009.06.004

Lay, T., Kanamori, H., & Ruff, L. (1982). The asperity model and the nature of large subduction zone earthquakes. *Earthquake Prediction Research*, *1*(1), 3–71.

Leeman, J., Scuderi, M. M., Marone, C., & Saffer, D. (2015). Stiffness evolution of granular layers and the origin of repetitive, slow, stick-slip frictional sliding. *Granular Matter*, *17*(4), 447–457. https://doi.org/10.1007/s10035-015-0565-1

Lewis, K. B., Collot, J.-Y., & Lallem, S. E. (1998). The dammed Hikurangi Trough: A channel-fed trench blocked by subducting seamounts and their wake avalanches (New Zealand–France GeodyNZ Project). *Basin Research*, *10*(4), 441–468. https://doi.org/10.1046/j.1365-2117.1998.00080.x

Lewis, K. B., Lallemand, S. E., & Carter, L. (2004). Collapse in a Quaternary shelf basin off East Cape, New Zealand: Evidence for passage of a subducted seamount inboard of the Ruatoria giant avalanche. *New Zealand Journal of Geology and Geophysics*, *47*(3), 415–429. https://doi.org/10.1080/00288306.2004.9515067

Lewis, K. B., & Pettinga, J. R. (1993). The emerging, imbricate frontal wedge of the Hikurangi margin. *Sedimentary Basins of the World*, *2*, 225–250.

Liu, Y., & Rice, J. R. (2007). Spontaneous and triggered aseismic deformation transients in a subduction fault model. *Journal of Geophysical Research*, *112*, B09404. https://doi.org/10.1029/2007JB004930

Lomax, A., Virieux, J., Volant, P., & Berge-Thierry, C. (2000). Probabilistic earthquake location in 3D and layered models. In C. H. Thurber & N. Rabinowitz (Eds.), *Advances in Seismic Event Location* (pp. 101–134). Netherlands: Springer. https://doi.org/10.1007/978-94-015-9536-0_5

McCausland, W. A., Creager, K. C., La Rocca, M., & Malone, S. D. (2010). Short-term and long-term tremor migration patterns of the Cascadia 2004 tremor and slow slip episode using small aperture seismic arrays. *Journal of Geophysical Research*, *115*, B00A24. https://doi.org/10.1029/2008JB006063

Mochizuki, K., Yamada, T., Shinohara, M., Yamanaka, Y., & Kanazawa, T. (2008). Weak interplate coupling by seamounts and repeating *M*~7 earthquakes. *Science*, *321*(5893), 1194–1197. https://doi.org/10.1126/science.1160250

Obara, K., Hirose, H., Yamamizu, F., & Kasahara, K. (2004). Episodic slow slip events accompanied by non-volcanic tremors in southwest Japan subduction zone. *Geophysical Research Letters*, *31*, L23602. https://doi.org/10.1029/2004GL020848

Obara, K., & Sekine, S. (2009). Characteristic activity and migration of episodic tremor and slow-slip events in central Japan. *Earth, Planets and Space*, *61*(7), 853–862. https://doi.org/10.1186/BF03353196

Ohta, Y., Freymueller, J. T., Hreinsdóttir, S., & Suito, H. (2006). A large slow slip event and the depth of the seismogenic zone in the south central Alaska subduction zone. *Earth and Planetary Science Letters*, *247*(1–2), 108–116. https://doi.org/10.1016/j.epsl.2006.05.013

Outerbridge, K. C., Dixon, T. H., Schwartz, S. Y., Walter, J. I., Protti, M., Gonzalez, V., et al. (2010). A tremor and slip event on the Cocos-Caribbean subduction zone as measured by a Global Positioning System (GPS) and seismic network on the Nicoya Peninsula, Costa Rica. *Journal of Geophysical Research*, *115*, B10408. https://doi.org/10.1029/2009JB006845

Ozawa, S., Miyazaki, S., Hatanaka, Y., Imakiire, T., Kaidzu, M., & Murakami, M. (2003). Characteristic silent earthquakes in the eastern part of the Boso peninsula, Central Japan. *Geophysical Research Letters*, *30*(6), 1283. https://doi.org/10.1029/2002GL016665

Pedley, K. L., Barnes, P. M., Pettinga, J. R., & Lewis, K. B. (2010). Seafloor structural geomorphic evolution of the accretionary frontal wedge in response to seamount subduction, Poverty Indentation, New Zealand. *Marine Geology*, *270*(1–4), 119–138. https://doi.org/10.1016/j.margeo.2009.11.006

Pelayo, A. M., & Wiens, D. A. (1992). Tsunami earthquakes: Slow thrust-faulting events in the accretionary wedge. *Journal of Geophysical Research*, *97*(B11), 15,321–15,337. https://doi.org/10.1029/92JB01305

Peng, Z., & Gomberg, J. (2010). An integrated perspective of the continuum between earthquakes and slow-slip phenomena. *Nature Geoscience*, *3*(9), 599–607. https://doi.org/10.1038/ngeo940

Peng, Z., Vidale, J. E., Wech, A. G., Nadeau, R. M., & Creager, K. C. (2009). Remote triggering of tremor along the San Andreas Fault in central California. *Journal of Geophysical Research*, *114*, B00A06. https://doi.org/10.1029/2008JB006049

Prejean, S. G., Hill, D. P., Brodsky, E. E., Hough, S. E., Johnston, M. J. S., Malone, S. D., et al. (2004). Remotely triggered seismicity on the United States West Coast following the M_w 7.9 Denali Fault earthquake. *Bulletin of the Seismological Society of America*, *94*(6B), S348–S359. https://doi.org/10.1785/0120040610

Protti, M., González, V., Kato, T., Iinuma, T., Miyazaki, S., Obana, K., et al. (2004). A creep event on the shallow interface of the Nicoya Peninsula, Costa Rica seismogenic zone. *AGU Fall Meeting Abstracts*, 41. Retrieved from http://adsabs.harvard.edu/abs/2004AGUFM.S41D..07P

Radiguet, M., Perfettini, H., Cotte, N., Gualandi, A., Valette, B., Kostoglodov, V., et al. (2016). Triggering of the 2014 M_w7.3 Papanoa earthquake by a slow slip event in Guerrero, Mexico. *Nature Geoscience*, *9*(11), 829–833. https://doi.org/10.1038/ngeo2817

Reyners, M., Eberhart-Phillips, D., & Stuart, G. (1999). A three-dimensional image of shallow subduction: Crustal structure of the Raukumara Peninsula, New Zealand. *Geophysical Journal International*, *137*(3), 873–890. https://doi.org/10.1046/j.1365-246x.1999.00842.x

Ruh, J. B., Sallarès, V., Ranero, C. R., & Gerya, T. (2016). Crustal deformation dynamics and stress evolution during seamount subduction: High-resolution 3-D numerical modeling. *Journal of Geophysical Research: Solid Earth*, *121*, 6880–6902. https://doi.org/10.1002/2016JB013250

Saffer, D. M., & Wallace, L. M. (2015). The frictional, hydrologic, metamorphic and thermal habitat of shallow slow earthquakes. *Nature Geoscience*, *8*(8), 594–600. https://doi.org/10.1038/ngeo2490

Schwartz, S. Y., & Rokosky, J. M. (2007). Slow slip events and seismic tremor at circum-Pacific subduction zones. *Reviews of Geophysics*, *45*, RG3004. https://doi.org/10.1029/2006RG000208

Segall, P., Rubin, A. M., Bradley, A. M., & Rice, J. R. (2010). Dilatant strengthening as a mechanism for slow slip events. *Journal of Geophysical Research*, *115*, B12305. https://doi.org/10.1029/2010JB007449

Shibazaki, B., & Iio, Y. (2003). On the physical mechanism of silent slip events along the deeper part of the seismogenic zone. *Geophysical Research Letters*, *30*(9), 1489. https://doi.org/10.1029/2003GL017047

Stein, R. S. (1999). The role of stress transfer in earthquake occurrence. *Nature*, *402*(6762), 605–609. https://doi.org/10.1038/45144

Stein, R. S., King, G. C. P., & Lin, J. (1992). Change in failure stress on the Southern San Andreas Fault System caused by the 1992 magnitude = 7.4 Landers earthquake. *Science*, *258*(5086), 1328–1332.

Stein, R. S., & Lisowski, M. (1983). The 1979 Homestead Valley earthquake sequence, California: Control of aftershocks and postseismic deformation. *Journal of Geophysical Research*, *88*(B8), 6477–6490. https://doi.org/10.1029/JB088iB08p06477

Toda, S., Stein, R. S., Reasenberg, P. A., Dieterich, J. H., & Yoshida, A. (1998). Stress transferred by the 1995 M_w = 6.9 Kobe, Japan, shock: Effect on aftershocks and future earthquake probabilities. *Journal of Geophysical Research*, *103*(B10), 24,543–24,565. https://doi.org/10.1029/98JB00765

Todd, E. K., & Schwartz, S. Y. (2016). Tectonic tremor along the northern Hikurangi Margin, New Zealand, between 2010 and 2015. *Journal of Geophysical Research: Solid Earth*, *121*, 8706–8719. https://doi.org/10.1002/2016JB013480

Vallée, M., Nocquet, J.-M., Battaglia, J., Font, Y., Segovia, M., Régnier, M., et al. (2013). Intense interface seismicity triggered by a shallow slow slip event in the Central Ecuador subduction zone. *Journal of Geophysical Research: Solid Earth*, *118*, 2965–2981. https://doi.org/10.1002/jgrb.50216

von Huene, R. (2008). When Seamounts Subduct. *Science*, *321*(5893), 1165–1166. https://doi.org/10.1126/science.1162868

Wallace, L. M., Barnes, P. M., Beavan, J., Van Dissen, R., Litchfield, N., Mountjoy, J., et al. (2012). The kinematics of a transition from subduction to strike-slip: An example from the central New Zealand plate boundary. *Journal of Geophysical Research*, *117*, B02405. https://doi.org/10.1029/2011JB008640

Wallace, L. M., & Beavan, J. (2010). Diverse slow slip behavior at the Hikurangi subduction margin, New Zealand. *Journal of Geophysical Research*, *115*, B12402. https://doi.org/10.1029/2010JB007717

Wallace, L. M., Beavan, J., Bannister, S., & Williams, C. (2012). Simultaneous long-term and short-term slow slip events at the Hikurangi subduction margin, New Zealand: Implications for processes that control slow slip event occurrence, duration, and migration. *Journal of Geophysical Research*, *117*, B11402. https://doi.org/10.1029/2012JB009489

Wallace, L. M., Beavan, J., McCaffrey, R., & Darby, D. (2004). Subduction zone coupling and tectonic block rotations in the North Island, New Zealand. *Journal of Geophysical Research*, *109*, B12406. https://doi.org/10.1029/2004JB003241

Wallace, L. M., Kaneko, Y., Hreinsdóttir, S., Hamling, I., Peng, Z., Bartlow, N., et al. (2017). Large-scale dynamic triggering of shallow slow slip enhanced by overlying sedimentary wedge. *Nature Geoscience*, *10*(10), 765–770. https://doi.org/10.1038/ngeo3021

Wallace, L. M., Reyners, M., Cochran, U., Bannister, S., Barnes, P. M., Berryman, K., et al. (2009). Characterizing the seismogenic zone of a major plate boundary subduction thrust: Hikurangi Margin, New Zealand. *Geochemistry, Geophysics, Geosystems*, *10*, Q10006. https://doi.org/10.1029/2009GC002610

Wallace, L. M., Webb, S. C., Ito, Y., Mochizuki, K., Hino, R., Henrys, S., et al. (2016). Slow slip near the trench at the Hikurangi subduction zone, New Zealand. *Science*, *352*(6286), 701–704. https://doi.org/10.1126/science.aaf2349

Wang, K., & Bilek, S. L. (2011). Do subducting seamounts generate or stop large earthquakes? *Geology*, *39*(9), 819–822. https://doi.org/10.1130/G31856.1

Wang, K., & Bilek, S. L. (2014). Invited review paper: Fault creep caused by subduction of rough seafloor relief. *Tectonophysics*, *610*, 1–24. https://doi.org/10.1016/j.tecto.2013.11.024

Wech, A. G., & Creager, K. C. (2008). Automated detection and location of Cascadia tremor. *Geophysical Research Letters*, *35*, L20302. https://doi.org/10.1029/2008GL035458

Wech, A. G., Creager, K. C., & Melbourne, T. I. (2009). Seismic and geodetic constraints on Cascadia slow slip. *Journal of Geophysical Research*, *114*, B10316. https://doi.org/10.1029/2008JB006090

Williams, C. A., Eberhart-Phillips, D., Bannister, S., Barker, D. H., Henrys, S., Reyners, M., & Sutherland, R. (2013). Revised interface geometry for the Hikurangi subduction zone, New Zealand. *Seismological Research Letters*, *84*(6), 1066–1073.

Wood, R., & Davy, B. (1994). The Hikurangi Plateau. *Marine Geology*, *118*(1–2), 153–173. https://doi.org/10.1016/0025-3227(94)90118-X

Yokota, Y., Ishikawa, T., Watanabe, S., Tashiro, T., & Asada, A. (2016). Seafloor geodetic constraints on interplate coupling of the Nankai Trough megathrust zone. *Nature*, *534*(7607), 374–377. https://doi.org/10.1038/nature17632

Zigone, D., Rivet, D., Radiguet, M., Campillo, M., Voisin, C., Cotte, N., et al. (2012). Triggering of tremors and slow slip event in Guerrero, Mexico, by the 2010 M_w 8.8 Maule, Chile, earthquake. *Journal of Geophysical Research*, *117*, B09304. https://doi.org/10.1029/2012JB009160